



## RESEARCH ARTICLE

10.1029/2021SW002953

### Special Section:

Space Weather Impacts on Electrically Grounded Systems at Earth's Surface

### Key Points:

- During storms, dB/dt spikes follow a general spatiotemporal development starting in the pre-midnight toward the morning sector
- Confirmation of 2 dB/dt hotspots (pre-midnight and morning sector) with different component characteristics independent of station location
- The peak value of Dst and AL indices during the entire storm is not correlated with the dB/dt spikes occurrence frequency of the storm

### Correspondence to:

A. Schillings,  
[audrey.schillings@space.umu.se](mailto:audrey.schillings@space.umu.se)







### Citation:

Schillings, A., Palin, L., Opgenoorth, H. J., Hamrin, M., Rosenqvist, L., Gjerloev, J. W., et al. (2022). Distribution and occurrence frequency of dB/dt spikes during magnetic storms 1980–2020. *Space Weather*, 20, e2021SW002953. <https://doi.org/10.1029/2021SW002953>

Received 14 OCT 2021

Accepted 7 APR 2022

# Distribution and Occurrence Frequency of dB/dt Spikes During Magnetic Storms 1980–2020

A. Schillings<sup>1,2</sup> , L. Palin<sup>3</sup> , H. J. Opgenoorth<sup>1,2</sup>, M. Hamrin<sup>1</sup> , L. Rosenqvist<sup>4</sup> , J. W. Gjerloev<sup>5,6</sup> , L. Juusola<sup>7</sup> , and R. Barnes<sup>5</sup>

<sup>1</sup>Department of Physics, Umeå University, Umeå, Sweden, <sup>2</sup>School of Physics and Astronomy, University of Leicester, Leicester, UK, <sup>3</sup>Toulouse, France, <sup>4</sup>Swedish Defence Research Agency, Stockholm, Sweden, <sup>5</sup>JHU/APL, Laurel, MD, USA, <sup>6</sup>Department of Physics and Technology, University of Bergen, Bergen, Norway, <sup>7</sup>Finnish Meteorological Institute, Helsinki, Finland

**Abstract** The physical magnetospheric cause for geomagnetically induced currents (GICs) are rapid time-varying magnetic fields (dB/dt), which occur mainly during magnetic substorms and storms. When, where and why exactly such rapid dB/dt may occur is insufficiently understood. We investigated all storms since 1980 and analyzed the negative and positive dB/dt spikes (>1500 nT/min) in the north and east component using a worldwide coverage (SuperMAG). Our analysis confirmed the existence of two dB/dt spikes “hotspots” located in the pre-midnight and in the morning magnetic local time sector, independently of the geographic location of the stations. The associated physical phenomena are probably substorm current wedge onsets and westward traveling surges (WTS) in the evening sector, and wave- or vortex-like current flows in the morning sector known as Omega bands. We observed a spatiotemporal evolution of the negative northern dB/dt spikes. The spikes initially occur in the pre-midnight sector, and then develop in time toward the morning sector. This spatiotemporal sequence is correlated with bursts in the AE index, and can be repeated several times throughout a storm. Finally, we investigated the peak value of Dst and AE during the storm period in comparison with the dB/dt spike occurrence frequency, we did not find any correlation. This result implies that a moderate storm with many spikes can be as (or more) dangerous for ground-based infrastructures than a major storm with fewer dB/dt spikes. Our findings regarding the physical causes and characteristics of dB/dt spikes may help to improve the GIC forecast for the affected regions.

**Plain Language Summary** Space weather prognosis is similar to meteorological weather but for predicting space events that can potentially damage humans technologies. One phenomenon are the geomagnetically induced currents or commonly called GICs. They are created by rapid fluctuations in the Earth's magnetic field, which can lead to power black outs and damages in communication systems. These rapid fluctuations are measured by worldwide magnetometers and defined as the time derivative of the magnetic field. In this study, we investigate the spikes in the time derivative for the two horizontal components, namely the northern and eastern component with a threshold of  $\pm 500$  nT/min. Our first result shows that these rapid fluctuations mainly occur in the magnetic local time (MLT) pre-midnight and morning sectors. We identified the possible physical phenomena that could caused the fluctuations. We also found that the spikes develop in space and time from the evening toward the morning MLT sectors. Finally, we found that a major geomagnetic storm does not necessary cause more spikes then a less intense one. Our findings concerning the physical nature of fast intense magnetic variations may help to improve the forecast of GICs.

## 1. Introduction

One of the most prominent (and potentially dangerous) features of space weather are geomagnetically induced currents, commonly known as GICs. The understanding of GICs is a major concern in order to preserve the power and communication systems and other technology on the ground. GICs are currents induced by rapid fluctuations in the Earth's magnetic field in any extended conducting technological infrastructure and can lead to malfunction or black outs of high-voltage power transmission systems (Pirjola & Boteler, 2002; Schrijver et al., 2015; Torta et al., 2012; Viljanen & Pirjola, 1994). To avoid and precisely forecast GICs, the scientific community introduced three warning levels for superstorms according to the magnetic index Dst and the intensity of the magnetic perturbation dB/dt associated with the auroral electrojet activity (Kataoka & Ngwira, 2016): the caution level for  $Dst \leq -300$  nT or  $dB/dt < -2,000$  nT/min, the warning level for  $Dst \leq -600$  nT or  $dB/dt < -4,000$  nT/min and the emergency level for  $Dst \leq -900$  nT or  $dB/dt < -6,000$  nT/min.

© 2022. The Authors.

This is an open access article under the terms of the [Creative Commons Attribution License](https://creativecommons.org/licenses/by/4.0/), which permits use, distribution and reproduction in any medium, provided the original work is properly cited.

The danger arises from rapid and sometimes extreme variations of  $dB/dt$ , which mainly occur during geomagnetic storms. Several famous super storms have resulted in strong GICs and power outage; the March 1989 storm provoked an electrical power black out in Quebec (Boteler, 2019), the Halloween storm in October 2003 also triggered a power black out over Sweden as well as in the UK due to geomagnetic disturbances of more than 400 nT/min (Erinmez et al., 2002; Kappenman, 2006; Wik et al., 2009). Extreme storms can also feature economic and social impacts if damages are deployed on satellites (Cannon et al., 2013). The intensity of a storm varies and its impact on Earth's environment is typically quantified by magnetic indices such as  $K_p$ , Dst (SYM-H) or AE index. The  $K_p$  index is a 3 hr index calculated with mid and high latitude magnetometers, the Dst (SYM-H) index has 1 hr (1 min) resolution and measures the enhancement of the equatorial ring current, and finally AE is a high latitude magnetic index with a resolution of 1 min and indicates the variation of electrojets in the auroral zone. Thus, a storm intensity with a  $Dst \leq -50$  nT is considered to be moderate, and intense for  $Dst \leq -100$  nT. It is defined as great storm for  $Dst \leq -250$  nT and as super storm for  $Dst \leq -500$  nT (Gonzalez et al., 1994, 2002; Lakhina & Tsurutani, 2016; Tsurutani et al., 1992).

During geomagnetic storms usually several substorms occur, but substorms do not necessary happen during a storm period (McPherron, 1997). Substorms are commonly identified using the magnetic AL and AU index because they are associated with decays and growths in the auroral electrojets and they lead to expanded aurora in the post-midnight region. The global phenomenon of magnetic storms is mainly associated with the large and varying ring current and therefore better characterized by indices like the Dst index. Both storms and substorms are consequences of interactions between the solar wind and the magnetosphere, often caused by a southward Interplanetary Magnetic Field (IMF). A long and continuous southward IMF typically triggers a storm in contrast to a weak and short southward IMF that creates a substorm (McPherron, 1997). During a substorm, it has been observed that magnetospheric particles are injected into the ring current and if this substorm injection process is quasi-continuous, it eventually leads to the main phase of a geomagnetic storm (Kamide et al., 1998; McPherron, 1997). Nevertheless, McPherron (1997) also suggested that a strong global convection could build up the ring current through a changing solar wind electric field rather than by substorm injection only. This hypothesis is supported by Wu et al. (2004), who studied auroral breakups at substorm onset and showed an uncorrelated occurrence relationship between storms and substorms.

The relationship between rapid magnetic variations in storms and substorms with GICs is relatively well known (Cannon et al., 2013; Kappenman, 2003; Pirjola, 2000; Pulkkinen et al., 2011). Any GIC caused by a  $dB/dt$  spike depend on its intensity, direction, spectral characteristics, the nature of the underlying three-dimensional conductivity in the ground and the geometry of any electric power network above the ground. Several studies recommend a frequency-weighted  $dB/dt$  in order to have a more precise proxy of GICs (e.g., Grawe et al., 2018; Heyns et al., 2021; Marshall et al., 2010; Pulkkinen et al., 2008; Rogers et al., 2021). The amplitude and phase of the geomagnetic spectrum has been shown to be important when determining the potential difference in oil pipeline (Marshall et al., 2010). Similarly, Heyns et al. (2021) studied the geomagnetic pulsations at mid-latitudes and found that low-frequency pulsations can lead to significant GICs. Thus, the GIC activity measured through  $dB/dt$  is biased in the low ultra-frequency range. On the other hand, Ngwira et al. (2013) and Thomson et al. (2011) argued that 60 s resolution for  $dB/dt$  is sufficient when investigating extreme storms. Thus, the occurrence frequency and characteristics of rapid geomagnetic variations, as well as exactly which physical parameters and drivers that potentially produce GICs is still not fully understood.

The dependency of interplanetary drivers and storm phases on magnetic variations has been studied by Kataoka and Pulkkinen (2008). The authors used the IMAGE magnetometer network data during CMEs (coronal mass ejections) and CIRs (co-rotating interaction regions) storms and provided a polar map, using the hourly maximum value, of the time derivative magnetic field behavior. Kataoka and Pulkkinen (2008) main result showed that the storm phase or the solar wind driver might influence the intensity and the location of the  $dB/dt$  spike values, which were mainly found along the midnight and morning sector of the auroral oval. The authors further established a power law relation between the  $dB/dt$  and GIC using IMAGE and power network GIC data in Scandinavia (Kataoka & Pulkkinen, 2008). Also based on the IMAGE network, Weigel et al. (2002) studied the relation between solar wind parameters and  $dB/dt$  (using a 30 min average) in order to predict GIC occurrences. They found two locations for  $dB/dt$  spikes up to several hundred nT/min; one in the pre-midnight sector and one in the pre-noon sector. The pre-midnight sector expands to lower latitudes due to substorm activity along the expanded auroral oval during intense storms (Weigel et al., 2002). The  $dB/dt$  events in the pre-noon sector was attributed

to ULF pulsations, which may be driven in that local time sector by Kelvin-Helmholtz instabilities (KHI) on the dawn flank magnetopause (Weigel et al., 2003). The authors identified these locations as the transition regions between eastward and westward electrojets (Weigel et al., 2002).

Many magnetic disturbances causing GICs are directly related to the time derivative of the equivalent ionospheric current density. Juusola et al. (2015) analyzed 10 s resolution data between 1994 and 2003 from the IMAGE magnetometer network and found that the most extreme equivalent current density variations happen in the dusk/pre-midnight and dawn sectors. In this case, the authors suggested that in the pre-midnight sector the events are related to substorm onsets and the westward traveling surge, in contrast to the dawn sector, where the responsible mechanism is probably related to eastward drifting large-scale auroral wave-features called Omega bands (Engebretson et al., 2020; Juusola et al., 2015; Opgenoorth et al., 1983, 1994). Other scientists (Kataoka & Pulkkinen, 2008; Ngwira et al., 2018; Pulkkinen & Kataoka, 2006) rather advocate Pc5 as potential cause for the observed disturbances in the morning sector.

We note that the above cited studies are based on data from the IMAGE network, which extends from 49.97° to 75.25° CGMLAT and covers only a limited sector of ~29° in longitude depending on the stations available. The available data cover only one magnetic local time (MLT) sector at one particular moment in the storm, and the statistical pattern obtained for different storms only stems from data when the local time sector happened to be over Scandinavia. In such way, a bias in the statistical distribution cannot be excluded, and the actual MLT distribution could be somewhat different.

Another study found two occurrence frequency maxima at pre-midnight and pre-noon sectors (EPRI, 2020). This study was based on two local magnetometer networks, which is an improvement to the above studies but does not provide full and simultaneous global coverage.

In this study, we focus on where and when large dB/dt disturbances, potentially leading to intense GICs, are more likely to happen. To some extent, we also address why these rapid variations happen. In contrast to all previous studies, we use global data from the SuperMAG database, which offers a good simultaneous coverage all over the world and we analyze geomagnetic data for all geomagnetic storms recorded with SYM-H < -100 nT since 1980. We then identify time and locations of any large (>1500 nT/min) temporal derivative of the north,  $B_N$ , and the east,  $B_E$ , components of the magnetic field and discuss our results in the Discussion (Section 4).

## 2. Method and Data Analysis

We used geomagnetic data from SuperMAG, a global magnetometers network (Gjerloev, 2012). The default SuperMAG coordinate system is NEZ, where N is positive in the direction of local magnetic north; E is positive in the local magnetic east direction; and Z is positive vertical down. For each storm, we used all the magnetometer stations available (all latitudes and longitudes combined) around Earth (data set—Schillings et al. [2021]). As we are interested in full global coverage since 1980, we downloaded data in 1-min resolution with all baselines subtracted (see SuperMAG website for further detail or Gjerloev [2012]). As complementary information for the storms, we also used the AE, Dst, and SYM-H indices and the Sudden Storm Commencement (SSC). When one or several SSCs were associated with a storm, we considered the first one as the onset of our studied storm.

In our analysis, we identified the spikes  $|dB_i/dt| \geq 1500$  nT/min (with  $i$  for north (N) or east (E)) in the north and east components separately using an automatic routine. In the automatic routine, a spike is defined by two consecutive data points with a value difference higher/lower or equal to  $\pm 500$  nT within 1 min. The restriction to 1 min data has some short-coming. First, we are not able to detect dB/dt spikes of 1500 nT/min or higher, which fall partially in two consecutive minutes. Second, we are not able to analyze more detailed spectral components in the variability of the magnetic field, which are known to have an impact on GIC occurrences (Grawe et al., 2018; Heyns et al., 2021; Marshall et al., 2010). On the other hand, the use of 1 min data allows us to study all storms in the last 40 years with an equivalent data set and a significant higher number of stations.

Figure 1 shows two examples of  $dB_N/dt$  spikes automatically detected at Dawson City (DAW—left panel) on 13 September 2005 at 07:49 and Daneborg (DNB—right panel) on 14 December 2006 at 23:45 stations. Figure 1a displays an example of a “good” spike, whereas Figure 1b is considered as a doubtful spike (see text below). Note that in our approach several successive 1 min spikes will in reality sum up to create a deeper sharpness in the magnetogram. However, as we used an automatic detection routine we chose to count all 1 min difference above

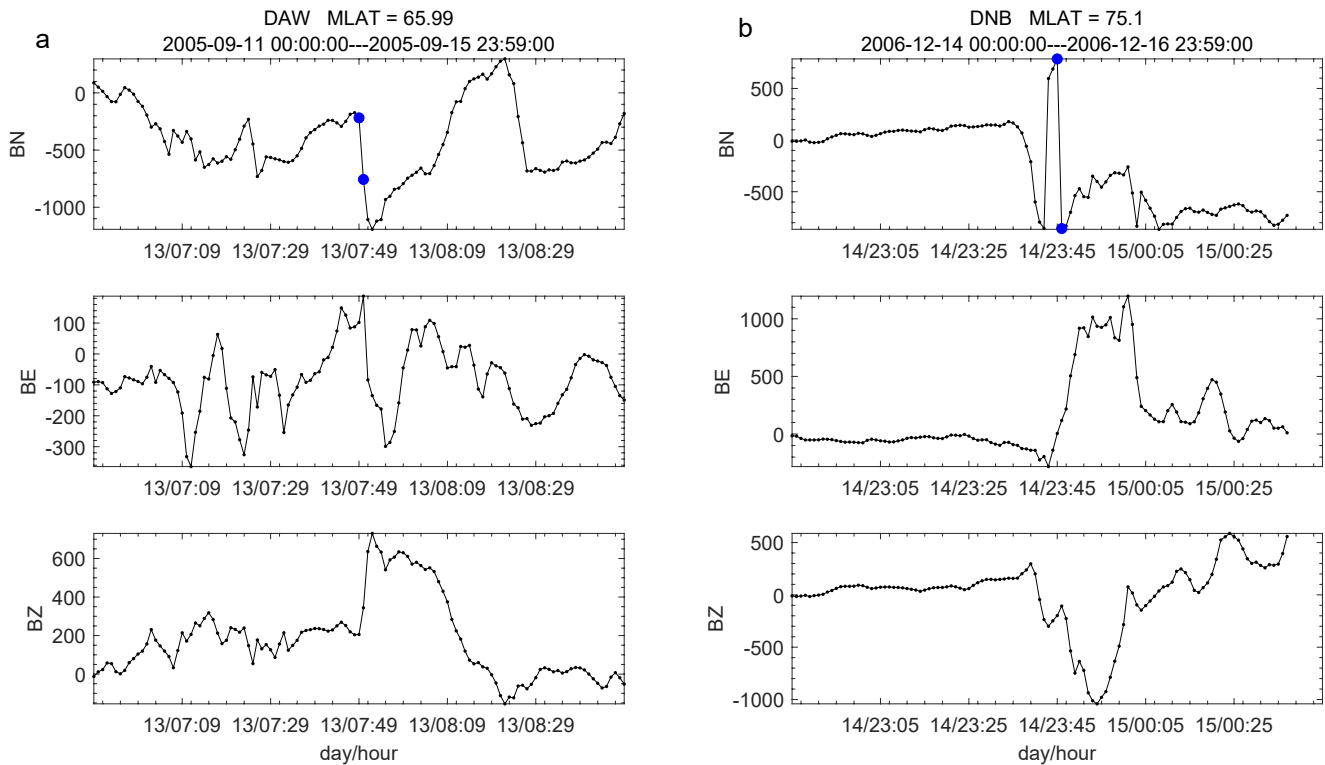


**Figure 1.** Examples of 1 min spikes ( $-dB_N/dt$ ) identified between the two blue dots. Panel (a) displays a spike identified as “good data” and is a moderate spike, whereas panel (b) shows an extreme, but “doubtful” spike ( $-dB_N/dt \leq -1,000$  nT/min). Note that  $B_E$  and  $B_Z$  are shown for comparison.

threshold separately. In Figure 1a, we present a spike for which the end of the negative magnetic excursion (13 September at 07:52) is not taken into account because the time derivative of the magnetic field for the following minute is less than the threshold (1500 nT/min). Potentially deep, but slow excursions may not fall within our categorization, because they are not sharp enough in their  $dB/dt$  effect. A better time resolution (e.g., 1 s or 10 s data) would clearly lead to the identification of many more events, but in the past and still today SuperMAG does not have many stations with that resolution available.

After automatic identifications of the spikes (such as shown in Figure 1), all the selected spikes have been visually inspected to avoid junk data and to identify whether the spikes are located close to a data gap or not. When a data gap is present in the magnetometer data, the  $dB/dt$  might be the result of magnetometer saturation in periods of high activity. In this case, the spike number and intensity might be underestimated. To better interpret the data, we classified them in three classes: (a) good data (see Figure 1a), (b) doubtful data (see Figure 1b), and (c) data just after a data gap. As doubtful data, we considered a significantly stronger (usually more than about 1800 nT) and almost symmetric  $dB/dt$  variation in one of the component but not in correlation (if any) with the two other components. The third class contains all spikes in  $dB/dt$  recorded within 3 min after the magnetogram showed missing data points (for several consecutive minutes) or in-between two data gaps. The first class with good data dominates the data set and only this class is used in our study.

In order to study the extreme geomagnetic disturbance potentially leading to GICs, we also divided the events into two categories based on the amplitude of the  $dB/dt$  spikes. The first category of spikes corresponds to  $1500 \leq |dB/dt| \leq 11,000$  nT/min (see Figure 1a) or moderate spikes, whereas the second category is for spikes  $|dB/dt| > 11,000$  nT/min or extreme spikes (see Figure 1b), where  $B_i$  can be either  $B_N$  or  $B_E$ . Thereafter, we refer to moderate or extreme spikes.

Our initial data set includes 307 storms between 1980 and October 2020 with SYM-H index below or equal to  $-100$  nT. These storms are selected from a storm list containing all identified storms (independently of SYM-H intensity) between 1980 and 2020 and has been created for this study by M. T. Walach and her team (see Walach and Grocott [2019] for further details about their algorithm). This list contains the extreme storms studied

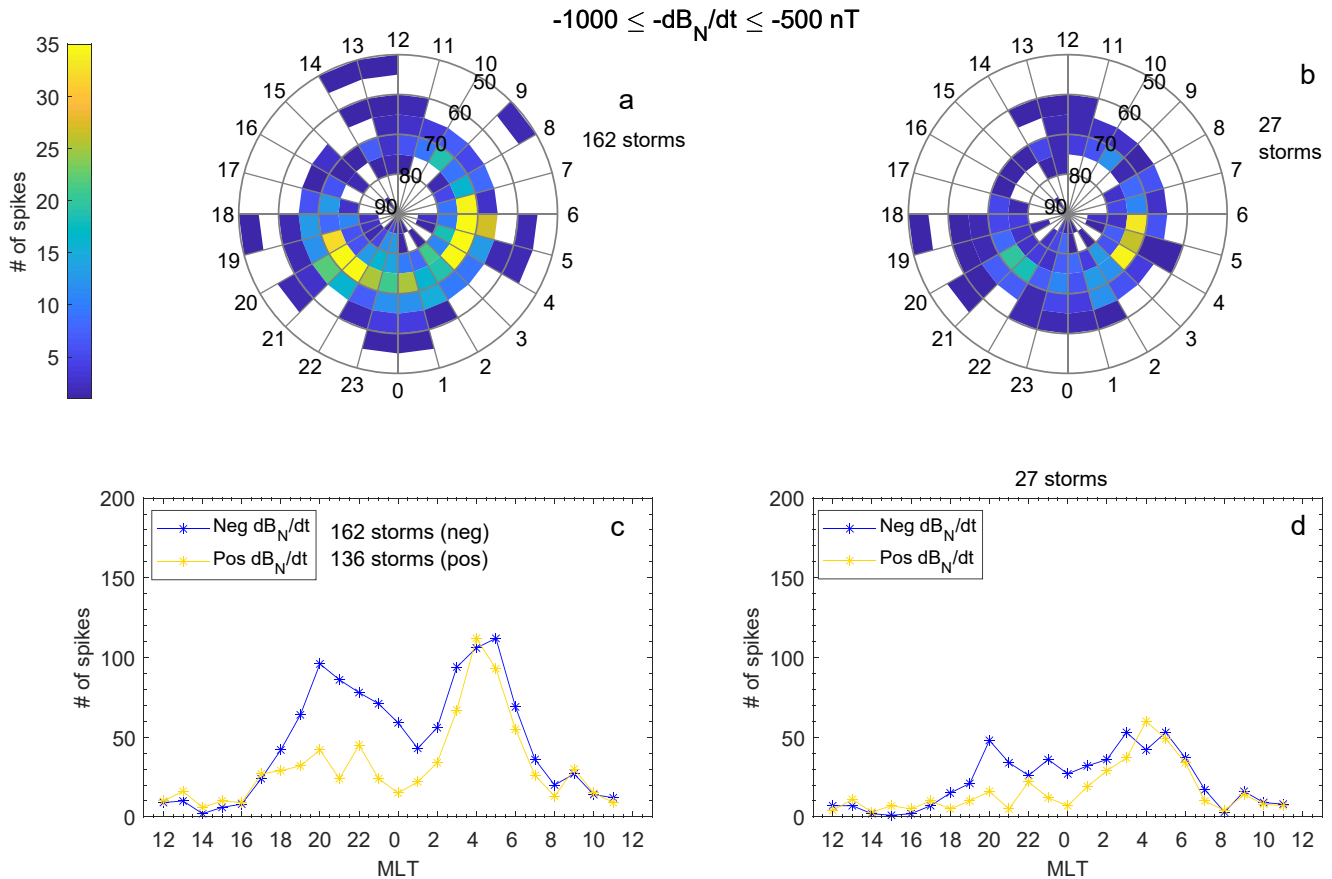


**Figure 2.**  $dB_N/dt$  in both hemispheres. The polar plots in panels (a) and (b) display the moderate spikes ( $-1,000 \leq dB_N/dt \leq -500$  nT/min) according to magnetic local time (MLT) and magnetic latitude. Panels (c) and (d) show the number of moderate spikes as function of MLT for  $-dB_N/dt$  in blue and for  $+dB_N/dt$  spikes in yellow. Panels (a) represent 162 storms (only  $-dB_N/dt$ ) and (c) represent 162 storms ( $-dB_N/dt$ —blue) and 136 storms ( $+dB_N/dt$ —yellow) with at least one  $dB/dt$  spike, whereas panels (b) and (d) show the same data but only for the 27 storms with more than 10 spikes.

previously, which can also be found for example, in Vennerström et al. (2016), Echer et al. (2008), and Zhang et al. (2007). We first investigate all  $dB/dt$  spikes found during the 307 storms (see Section 3.1—two popular “hotspots”). To obtain relevant statistics and to further study the spatiotemporal development of  $dB/dt$  disturbances during the individual storms, we then selected only storms with more than 10  $dB/dt$  spikes. The 10 spikes must be recorded at three different stations at least. We found that from the 307 storms, 162 (136) have at least one detected  $-dB_N/dt$  ( $+dB_N/dt$ ) spike and 153 (137) have at least one detected  $-dB_E/dt$  ( $+dB_E/dt$ ) spike. Merely 27 fulfill the further conditions of 10 spikes during the storm. All storms except 3, have one (or several) associated SSC in the preceding 36 hr before the first detected spike above our chosen threshold.

### 3. Observations and Results

#### 3.1. Confirmation of Two Popular “Hotspots” for $dB/dt$ Spikes: Pre-Midnight and Morning Sectors

For both hemispheres, we identified the negative and positive deviations ( $|dB/dt| \geq 1500$  nT/min) of the magnetic north and east components for all stations and determined their corresponding MLT and magnetic latitude (MLat). Due to similarities in the hemispheres (Viljanen & Tanskanen, 2013), Figure 2a shows the results for all 162 storms for the negative moderate spikes or  $-dB_N/dt$  in both hemispheres, whereas Figure 2b shows the same data but only for the 27 storms with more than 10 detected spikes. The polar plot displays the spike occurrence as a function of MLT (0–23) on the radii, with noon on the top and midnight at the bottom, while the concentric circles represent the MLat ( $90^\circ$ – $50^\circ$  starting from the pole). The color bar indicates the number of identified spikes within every 1 hr MLT and  $5^\circ$  MLat bin, and we display only the data for the spikes classified as “good” (see Section 2 for the classes). In Figures 2c and 2d, we present the total number of detected (moderate) spikes



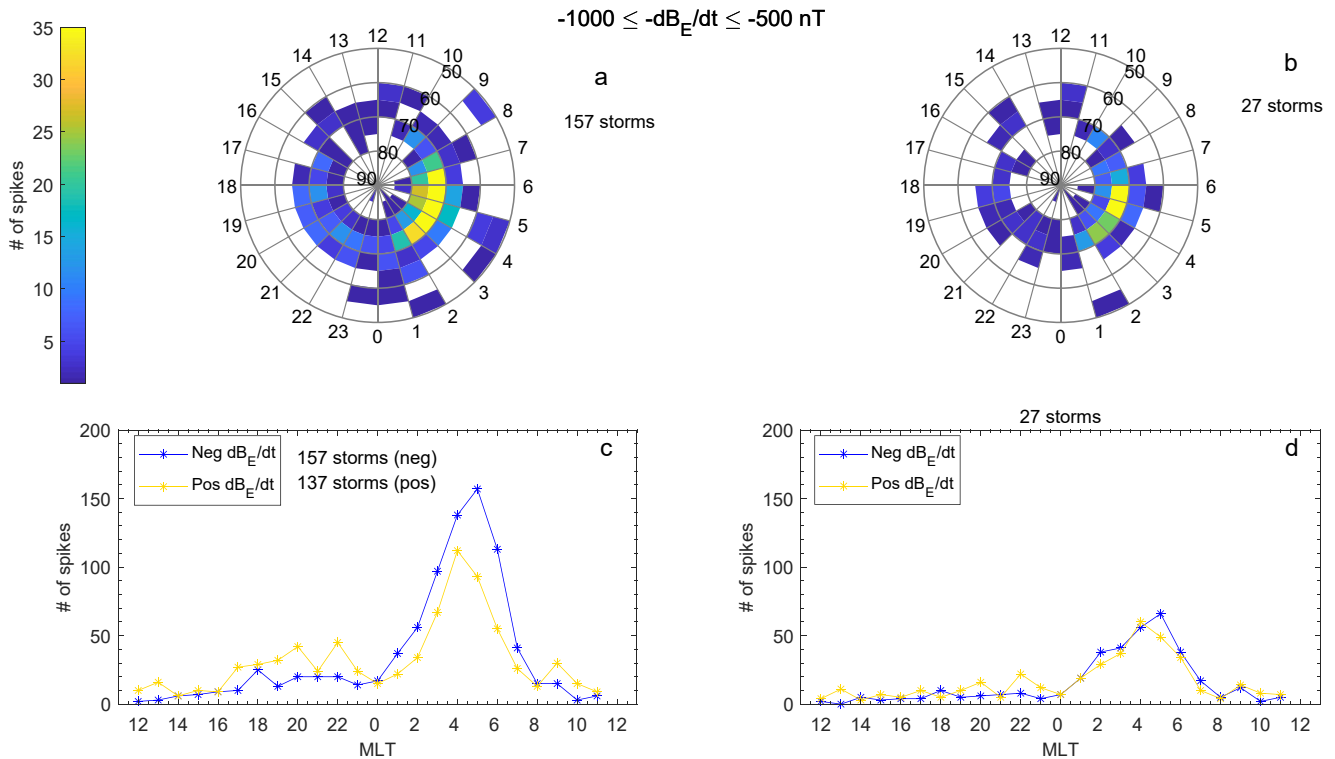


**Figure 3.** Similar as Figure 2 for the eastern component of the magnetic field or  $dB_E/dt$ .

versus MLT in both the negative and positive component  $dB_N/dt$  with the blue and yellow solid lines, respectively. In the polar plots (Figures 2a and 2b), we observe a clear distribution of the moderate spikes along the entire nightside ( $\sim 20\text{--}06$  MLT) auroral oval ( $\sim 65^\circ\text{--}75^\circ$  MLat), extending slightly into the post dawn sector. The spikes in  $-dB_N/dt$  (see Figures 2a and 2b) have two distinct occurrence maxima, one in the pre-midnight sector around 21 MLT and one centered around 04–05 MLT in the morning sector. This double peaked distribution becomes clearer in the corresponding blue line in panels (c and d). We note that the morning sector maximum exhibits almost the same number of positive ( $dB_N/dt$ ) events (yellow line) as negative ones, while the pre-midnight sector is clearly dominated by negative spikes for all storms in panel (c) as well as the 27 storms only in panel (d).

In Figure 3 showing the eastern component or  $dB_E/dt$ , we also see the  $dB/dt$  spike distribution along the auroral oval but only in the morning sector. In this sector between 02 and 07 MLT, we observe a clear increased occurrence frequency for both positive and negative spikes, centered at 04–05 MLT as for the northern component, and located well within the auroral zone. The pre-midnight maximum, which is observed mostly for the negative spikes of the northern component in Figures 2c and 2d does not exist in the eastern component (see Figures 3c and 3d). An exception of a slight increased occurrence frequency is however observed for positive  $dB_E/dt$  spikes between 20 and 22 MLT (yellow line in Figures 3c and 3d). We will come back to this interesting observation in discussion Section 4. We also analyzed both components for the extreme spikes (data not shown) but those  $dB/dt$  spikes are rare and they do not seem to occur in any specific MLT sector.

In summary, we confirmed two clear occurrence maxima for the observed spikes in  $dB/dt$  during all storms for a worldwide coverage: a pre-midnight hotspot for mainly the negative  $dB_N/dt$  and a morning hotspot for negative and positive spikes in both the  $dB_N/dt$  and  $dB_E/dt$  components. In the morning sector, the occurrence frequency of positive and negative spikes of the eastward component (see Figure 3c) is larger than in the northward component (see Figure 2c). The pre-midnight sector hotspot does not exist for spikes in the eastward component. As we discuss in the discussion Section 4, our observations indicate that the pre-midnight sector hotspot appears to be mainly related to intensification of the westward electrojet (negative  $B_N$ ), while in the morning sector spikes can occur in basically any component, with some preference for the eastward component, that is, both north or southward directed current enhancements.

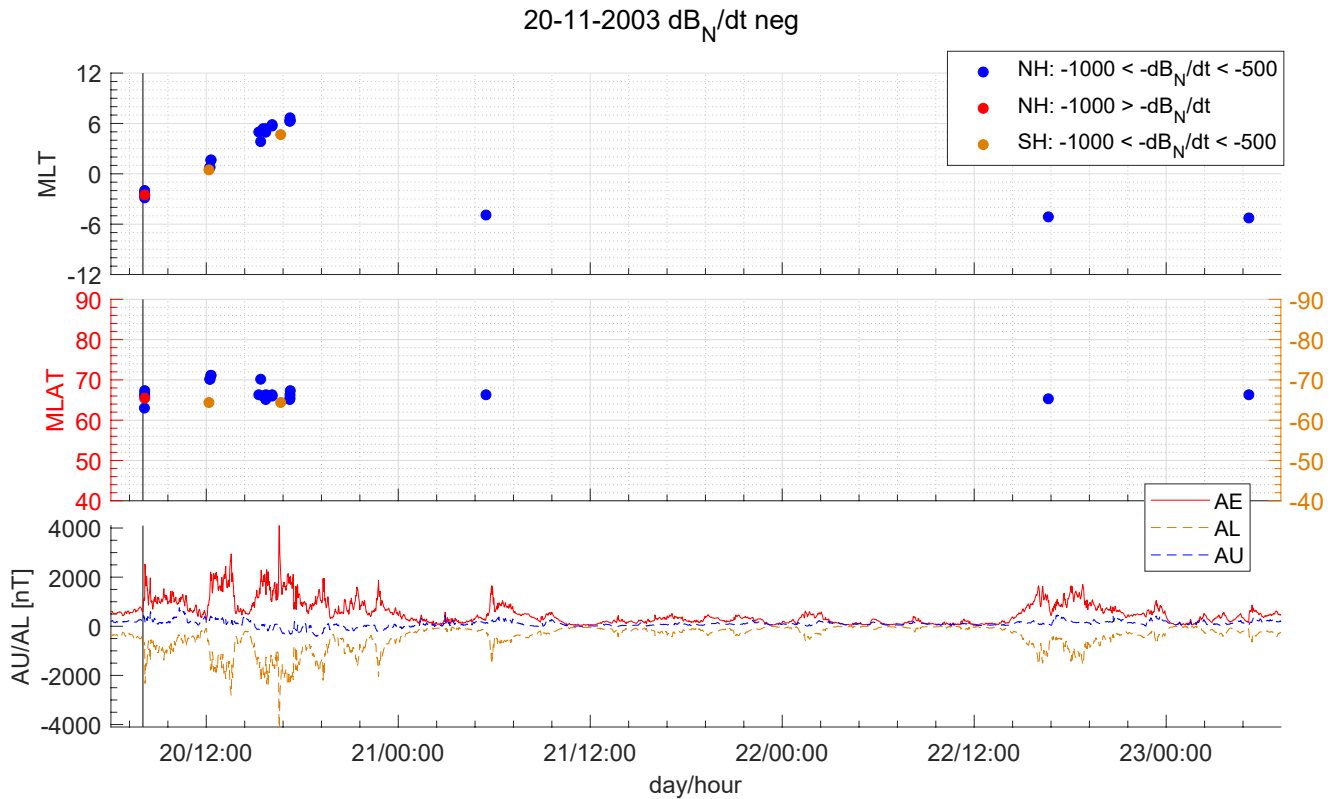


**Figure 4.** Spikes for  $-dB_N/dt$  in both hemispheres during the 20 November 2003 storm. The top and middle panels present the moderate (blue dots in the NH and orange dots in the SH) and extreme (red dots in the NH) spikes according to the magnetic local time and magnetic latitude respectively, while the bottom panel shows the corresponding AE (AU/AL) index. The black solid line corresponds to the associated Sudden Storm Commencement. NH and SH in the legend stand for northern and southern hemisphere respectively.

### 3.2. Spatiotemporal Evolution of the Spikes During the Storms

To further investigate the character of the spike occurrences, we studied the spatiotemporal development of the spikes for the 27 storms having more than 10 identified spikes. In order to have a general picture of each of these disturbed periods, we analyzed the solar wind (not shown), the auroral electrojet indices (AE, AU, AL) and the associated SSC for each storm. We observe a common tendency for almost all storms: the first spikes occurred in the evening or pre-midnight sector and develop later in time toward the morning sector. We present two typical examples of  $-dB_N/dt$  spikes; the storm of the 20 November 2003 in Figure 4 and the 8 February 1986 storm in Figure 5. In both figures, the top, middle and bottom panels show the MLT, the MLat and the index respectively as a function of time (day/hour—DD/HH:MM). Note that in the middle panel, the left y-axis (red) shows the northern hemisphere (NH) MLat, whereas the right y-axis (orange) shows the southern hemisphere (SH) MLat. The full colored dots correspond to the spikes of different intensity and in the NH (SH): blue (orange) spikes have a value between  $-1,000$  and  $-500$  nT and red spikes are below  $-1,000$  nT.

The 20 November 2003 started with an SSC that occurred on 20 November at 08:02 UT (vertical black solid lines in Figure 4). In the 10 min following the SSC, four moderate (blue dots) and one extreme (red)  $-dB_N/dt$  spikes were recorded by magnetometers in the auroral oval and all of them are from ionospheric origin (visually checked—SSC spikes are characterized by their pattern looking as a sharp and squeezed Z letter in the horizontal position). The spikes occurred between 21 and 22 MLT so that the pre-midnight sector has been activated right after the SSC. Once the magnetic activity ceases in the midnight sector, the post-midnight sector is activated and we observe four moderate spikes (blue dots) in the NH and one spike in the SH (orange dot) as shown in Figure 4 on 20 Nov around 12:00 UT. A few hours after the activation of the post-midnight sector, the morning sector (05–06 MLT) is activated with 12  $-dB_N/dt$  spikes in both hemispheres. This spatiotemporal development of  $-dB_N/dt$  spikes is clearly visible in Figure 4 top panel. The  $dB/dt$  spikes take place during the initial and main phase

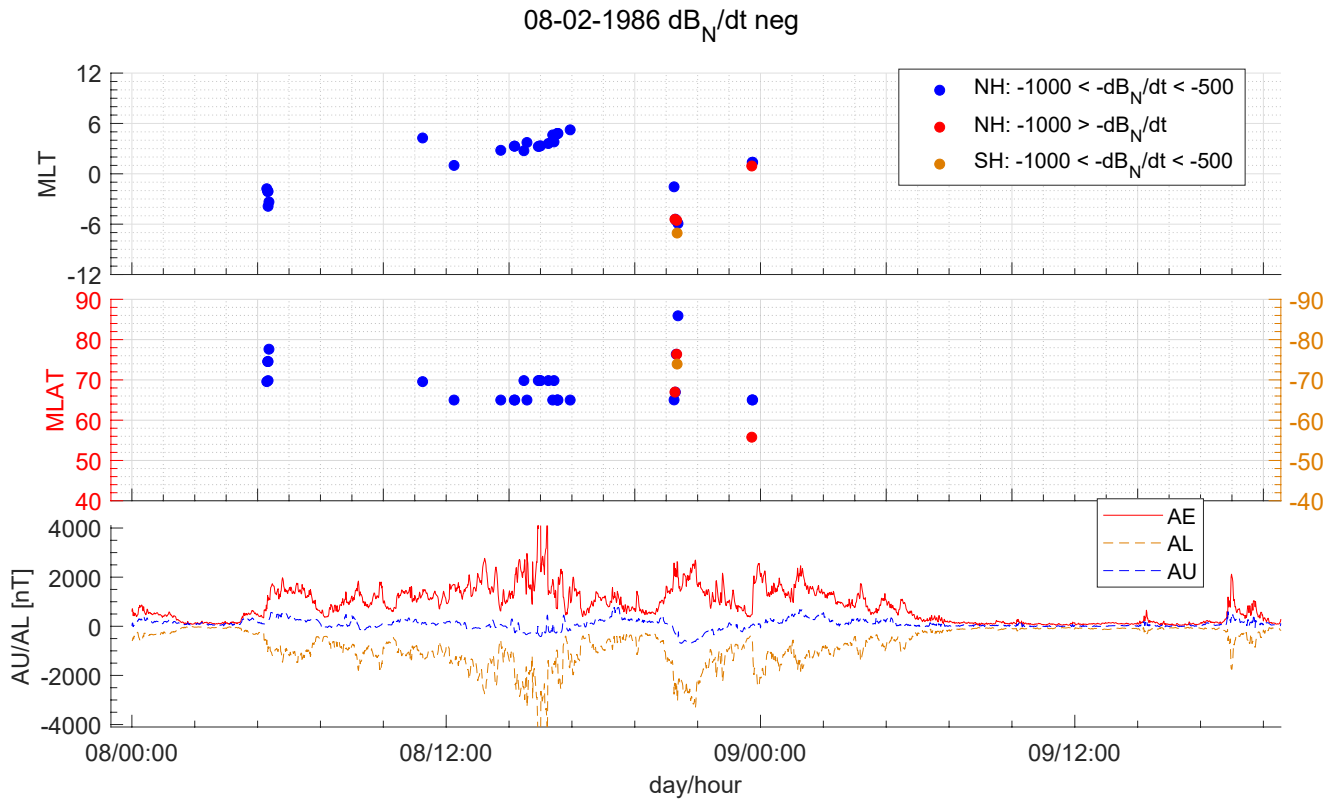


**Figure 5.** Similar as Figure 4 for the 8 February 1986 storm. Note that the associated Sudden Storm Commencement occurred on 6 February 1986 at 13:12 UT (not shown).

of the geomagnetic storm. Note that the few later spikes occurred in the storm recovery phase and are probably caused by the enhancement of the auroral electrojet due to minor substorms.

Our second example is shown in Figure 5. The storm happened on 8 February 1986, it had one associated SSC on 6 February at 13:12 UT (not shown for clarity reason) and very few available solar wind data during the storm period. The auroral electrojet (AE index) shows a clear enhancement on 8 February at 05:00 UT associated with 5  $-dB_N/dt$  spikes (in the NH) observed in the evening sector. Later in the storm (starts at 11:06—8 February) the post-midnight and finally the morning sector were activated with a peak value in the AE index of 5,220 nT. In the top panel of Figure 5, we clearly see the same spatiotemporal evolution of the  $-dB_N/dt$  spikes; following the initial intensification of the pre-midnight sector, the morning sector gets active first around 03 MLT at about 14:00 UT, and a sequence of spikes developed further and further into the morning sector, ending with the last spike around 06 MLT at about 17:00 UT. A second intensification of the magnetic storm occurred around 21:00 UT (8 February 1986) predominantly all along the evening sector with several extreme spikes in the NH. About 3 hrs later (midnight in UT), new spikes were detected in the post-midnight sector, again following the same temporal development described above. Thus, we have two clear spatiotemporal development of the  $-dB_N/dt$  spikes for this storm in 1986.

Every geomagnetic storm has its own distinctive features, and are often composed of several intensifications which are due to the different structure of the solar wind drivers for each event. We could find similar trends—first spikes observed in the evening sector after intensification, later on spikes are located around midnight and finally in the morning sector—in the majority of the 27 storms. However, there are some noteworthy exceptions that we like to present. Particular exceptions include major geomagnetic storms, such as the Halloween event on 29 October 2003, for which we observe some spikes in the afternoon sector. In contrast, for some moderate geomagnetic storms, the initial onset activation around the pre-midnight sector can be lacking, or these onset spikes could be below the detection level. We discuss these exceptions in further detail in the Discussion Section 4.



## 4. Discussion

### 4.1. Ionospheric Phenomena Related to the Hotspots

We studied the occurrence pattern of  $dB/dt$  spikes in both the northward and eastward magnetic component for 307 storms over 40 years, as well as for a subset of 27 storms with more than 10 spikes. In Figures 2 and 3, we found two distinctive hotspots, one pre-midnight and one close to dawn where  $dB/dt$  spikes occurred in either the northern or eastern component. In previous studies (EPRI, 2020; Juusola et al., 2015; Kataoka & Pulkkinen, 2008; Viljanen et al., 2001; Weigel et al., 2002) these particular locations where  $dB/dt$  spikes occur more frequently have already been discussed with various conclusions, but none of these studies used data with a simultaneous worldwide coverage. Our result shows without observational bias that rapid variations are most likely to occur in the pre-midnight and dawn sectors, independently of the station locations in any particular storm.

The pre-midnight hotspot features mostly negative  $dB_N/dt$  spikes and with a lower occurrence for the positive ones (see Figures 2a and 2c). In the pre-midnight sector along the auroral oval, the negative (and few positive)  $dB_N/dt$  spikes are most probably caused by sudden enhancements of the westward (eastward) electrojets. A large number of both statistical and case studies have shown that the onset of westward electrojet enhancements typically stems from the formation of a substorm current wedge (SCW), associated with magnetospheric plasma flow bursts entering the inner edge of the magnetotail plasma sheet (Juusola et al., 2015; Kepko et al., 2015; Lyons et al., 2013; Palin et al., 2015, 2016).

The SCW onset results from a pair of upward (on the western edge) and downward (on the eastern edge) field-aligned currents (FAC), connected by a narrow and intense westward substorm electrojet (Kepko et al., 2015; McPherron et al., 1973). In optical emissions the SCW is associated with an abrupt brightening and poleward expansion of auroral arcs (Kepko et al., 2015; Kisabeth & Rostoker, 1973). After the onset, this SCW develops into a poleward bulge from the aurora feature, and its western edge which is characterized by the localized upward FAC, develops finally into an auroral surge. This auroral surge moves westward (and poleward) as the SCW expands in all directions. This newly born feature, located on the western edge of the SCW and traveling toward west more or less along the auroral oval is called westward traveling surge (WTS; Ebihara & Tanaka, 2018; Tighe & Rostoker, 1981). WTS has an important magnetic effect on the ground, characterized by a localized counterclockwise Hall-current loop, the strongest features of which are a negative northern component magnetic field  $B_N$  poleward of the surge and a positive eastern component  $B_E$  on the western edge of the surge (Oppe-noorth et al., 1983). We suggest that these enhancements result in the most prominent  $dB/dt$  spikes (in both components) that we observed in the evening/pre-midnight sector. The broad occurrence peak of negative  $dB_N/dt$  shown in Figure 2c is interpreted as part of the magnetic signature of SCW onset(s) close to the observing stations (many negative  $dB_N/dt$  spikes). We also found a small population of only positive  $dB_E/dt$  spikes in the pre-midnight hotspot (Figures 3c and 3d). A detailed analysis indicated (data not shown) that this population is exclusively associated with WTS during the Halloween storm (October 2003) and its spikes discussed in the next Section 4.2. During the Halloween storm, some observing stations may just happen to be located at the western edge of the SCW then allowing for the observation of WTS signatures (fewer observations of positive  $dB_E/dt$  in a much narrower MLT sector; for further details, see also Kepko et al. [2015] Figure 13b). This result agrees with Viljanen et al. (2001), who suggested that localized ionospheric current structures might play an important role for GIC development in addition to the main electrojet.

The second hotspot in the morning sector includes observations of negative and positive  $dB/dt$  spikes from both horizontal magnetic components (N and E) with more or less similar occurrence frequencies (a maximum of about 70 per MLT bin) for the 27 storms (see Figures 2d and 3d). In contrast, the statistics for all storms show a higher occurrence frequency of  $dB_E/dt$  spikes (a maximum of about 170 per MLT bin) compared to  $dB_N/dt$  spikes (a maximum of about 110 per MLT bin). This asymmetry may indicate that in the morning sector hotspot the observed variability of the ionospheric current flow is more often caused by north-south directed current enhancements ( $B_E$ ), while similar enhancements (alternatively depletions) in the east/west electrojet ( $B_N$ ) are about 35% less commonly observed. In summary, we note that in the morning sector hotspot sudden intensification of the ionospheric current deviations (strong  $dB/dt$ ) can occur in all four directions (north, south, east and west), which in our understanding immediately brings into mind the currents and the associated magnetic features of traveling vortices.

Thus, we conclude that the observed variety of dB/dt spikes in the early morning to dawn sector might be caused by very different processes compared to the spikes observed in the pre-midnight sector. In the morning sector, there exist several known auroral and ionospheric current features, which are typically connected to the recovery phase of both substorms and storms, but probably occupying different MLT sectors. In the literature (Apatenkov et al., 2020; Engebretson et al., 2020; Opgenoorth et al., 1983, 1994; Partamies et al., 2017), any dB/dt spikes in the post-midnight (02–04 MLT) sector are most likely associated with the signatures of field aligned and ionospheric current flow in Omega bands. The physical mechanism behind Omega bands is a current instability drifting eastward in the Region 1 current and forming large-scale auroral wave-forms in the shape of the (inverse) Greek letter Omega. They are associated with so-called magnetic Ps6 (Pi5) pulsations (Kleimenova et al., 2018; Pulkkinen & Kataoka, 2006; Viljanen et al., 2001; Yagova et al., 2018) and are frequently observed by satellites and all-sky cameras. In their statistics of auroral Omega bands, Partamies et al. (2017) showed that a certain threshold level of magnetic activity (more than the average) is required for the Omega bands to form. Statistically, Partamies et al. (2017) and Apatenkov et al. (2020) found that Omega bands are typically observed at about 02–03 MLT, and mostly in the recovery phase of major substorms. However, the authors showed that Omega band signatures can also be observed until 07 MLT, which is in agreement with our morning sector dB/dt spike observations.

Some authors suggested that dB/dt spikes in the local morning sector could alternatively be associated with Pc5 pulsations generated by the Kelvin-Helmholtz instability (KHI; Kataoka et al., 2001; Ngwira et al., 2018; Pulkkinen & Kataoka, 2006; Weigel et al., 2003) or by upstream ion-cyclotron resonance (Howard & Menk, 2005) on the morning flank of the magnetopause. However, we do not believe this explanation because any processes at the magnetopause, including KHI (independently of their scale), would magnetically map very close to the vicinity of the dayside cusp, that is, not much further than 08–09 MLT into the dawn sector, as the longitudinal variability of the cusp in response to solar wind forcing is not more than three to maximum of 4 hr from local noon (Pitout & Bogdanova, 2021). Thus, it appears very difficult to connect the ionospheric current features caused by the KHI at the flanks with our observations in the morning sector at 05–06 MLT. At this MLT, the excessive compression in the mapping of magnetopause signatures to the ionosphere, KHI may also not be able to explain the large-scale signatures (500–1,000 km) of the morning sector current-structures observed.

#### 4.2. Spatiotemporal Development: Case Studies of 13 July 1982 and 29 October 2003

We have shown in the Observations Section 3.2 that the typical spatiotemporal development of storms usually starts after a storm onset, that is, an SSC (if one is recorded), and that the location of increased occurrence frequency of spikes shows a spatial development from the pre-midnight toward the dawn sector. A storm period can have several intensifications, after each of which the entire sequence starts again from pre-midnight onward toward the dawn. Since every storm has its own particular onset(s) and multiple intensifications, which most certainly depend on the particular structure of its solar wind drivers, we discuss two cases that do not exactly follow the general tendency: the storm on 13 July 1982 and the so-called Halloween storm on 29 October 2003.

Figure 6 displays the 13 July 1982 storm associated with a SSC on 13 July at 16:18 UT, however, all 15 dB/dt spikes during this storm are observed only about 24 hrs later, starting right before midnight (UT) on 14 July. Surprisingly, the spikes are spread out over most of the MLT range and from 50° to 80° Mlat within 1 hr (first spike at 23:19 UT and last one at 00:31 UT). We observe a “shifted” temporal evolution with the start (first spike of sequence would be the blue dot—arrow on the top panel in Figure 6) occurring in post-midnight instead of in the evening sector and then evolving toward morning. The dB/dt spikes in the post-midnight sector are recorded at a latitude southward of the auroral zone (see squared blue dots in the top panel), this may explain the shift of the initial dB/dt spikes MLT location toward and beyond midnight. Around UT midnight (00:00 UT on 14 July), we observe another unusual feature; seven dB/dt spikes were detected at basically all MLT locations between –11.2 and 11.87 MLT within only 6 min (23:53 UT to 23:59 UT). These spikes observed along the entire 24 hr MLT range occurred simultaneously with a significant sudden decrease in the AL index: from –1,473 nT at 23:53 UT to –3,033 nT at 00:01 UT. According to SYM-H index (not shown), this 6 min interval corresponds to the potential main phase of the storm. This particular case shows that a possible explanation such as a local release of the magnetospheric stored energy close to midnight (substorm analogy) does not always fit to explain the latitude and MLT development of the dB/dt spikes. The spikes can indeed happen anywhere for yet unclear reasons.

Another exception to the spatiotemporal development we discussed previously is the Halloween storm on 29 October 2003 shown in Figure 7. This storm is particular because it features an incredible amount of 218 dB/dt

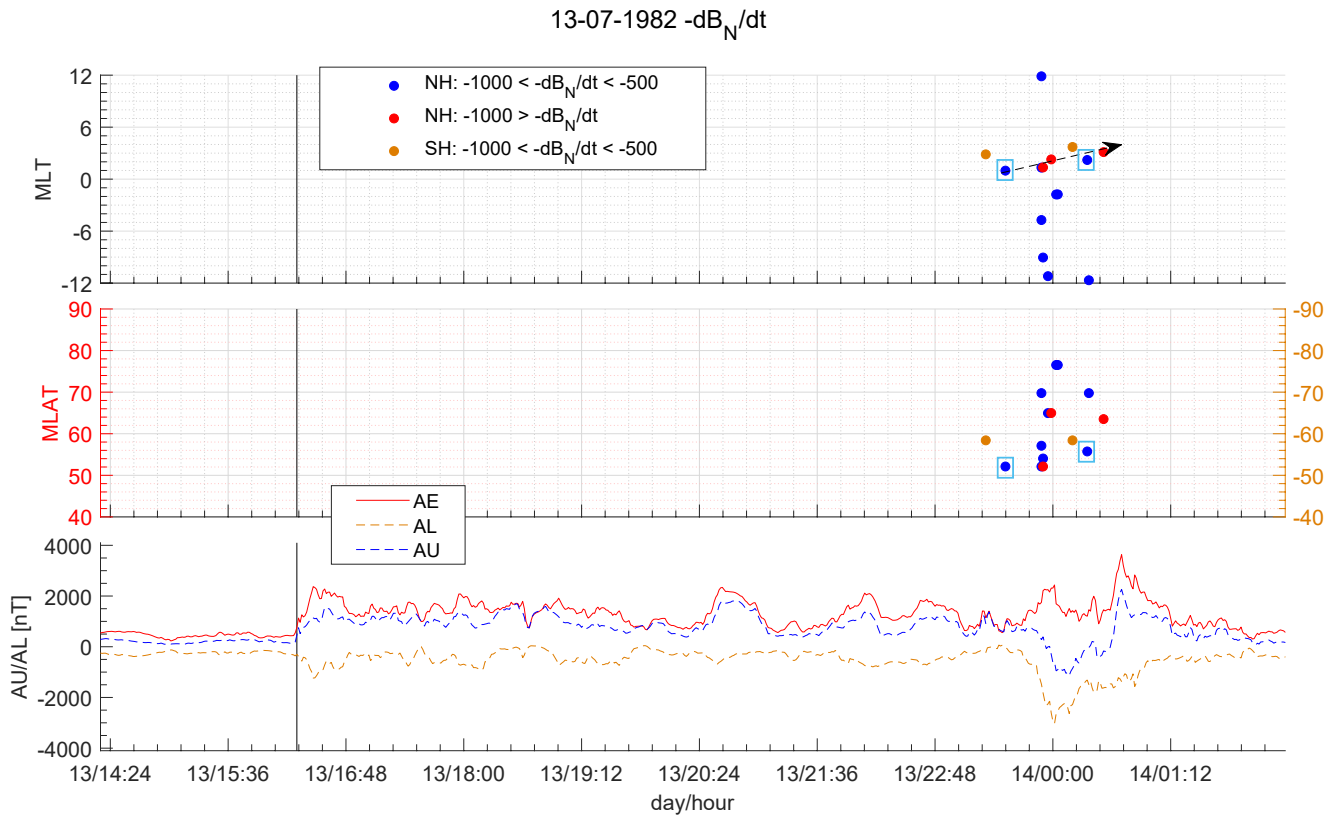


**Figure 6.** Similar as Figure 4 for the 13 July 1982 storm. The arrow shows the late start of the spatiotemporal sequence for this storm considered as one exception to the general spatiotemporal tendency observed in Figure 4 or Figure 5 (further detail in the text). The squared blue dots show the unusual low latitudes of the spike observations.

dt spikes (by far the largest number detected in any of the storms we studied). The spikes were detected by 63 different magnetometer stations worldwide within 48 hr. The storm is associated with three SSCs (only two are shown in Figure 7) on 26, 28, and 29 October, respectively. The last one occurred on 29 October at 06:10 UT and triggered a magnetic activity between  $50^\circ$  and  $90^\circ$  MLat as well as in almost all MLT ranges. Right after the third SSC between 06:10 UT and 07:20 UT, 95 spikes were detected from the early evening sector  $-5.4$  MLT to late morning sector  $9.2$  MLT. If we isolate these  $dB/dt$  spikes, we do find a similar “shifted” spatiotemporal development (not shown and not visible in Figure 7 due to the amount of spikes), however, it is relatively short in time compared to other storms and some other MLT sectors were activated almost simultaneously, which make the trend less clear. Many of the ionospheric and magnetospheric phenomena related to the “Halloween”  $dB/dt$  spikes have not yet been investigated in depth, but the large number of the spikes certainly contributes to the statistical polar plots shown in all panels of Figures 2 and 3.

### 4.3. Spatial Distribution of the SuperMAG Stations

Despite previous observations, one may think that the spikes in the pre-midnight and then in the morning MLT sector could be related to when and over which region the storm starts. That hypothesis was not verified when we plotted individual maps with the geographical coordinates of the stations that recorded the  $dB/dt$  spikes. In addition, if some  $dB/dt$  spikes in the pre-midnight have been observed by European stations, the following  $dB/dt$  spikes in the spatiotemporal relation might occur over Canada, at a later time when Europe has rotated into the dayside and Canada is located in the morning sector. We did not find any logical or coherent trend neither between the storm start and the corresponding hotspot nor between the location of the stations and the occurrence frequency in the MLT sector. Figure 8 displays all stations that recorded at least one  $dB/dt$  spike for the 27 storms. The blue and orange stars represent stations that recorded  $-1,000 \leq dB_N/dt \leq -500$  nT/min in the NH and SH respectively and similarly the red (NH) and magenta (SH) stars represent stations that recorded  $dB_N/dt$

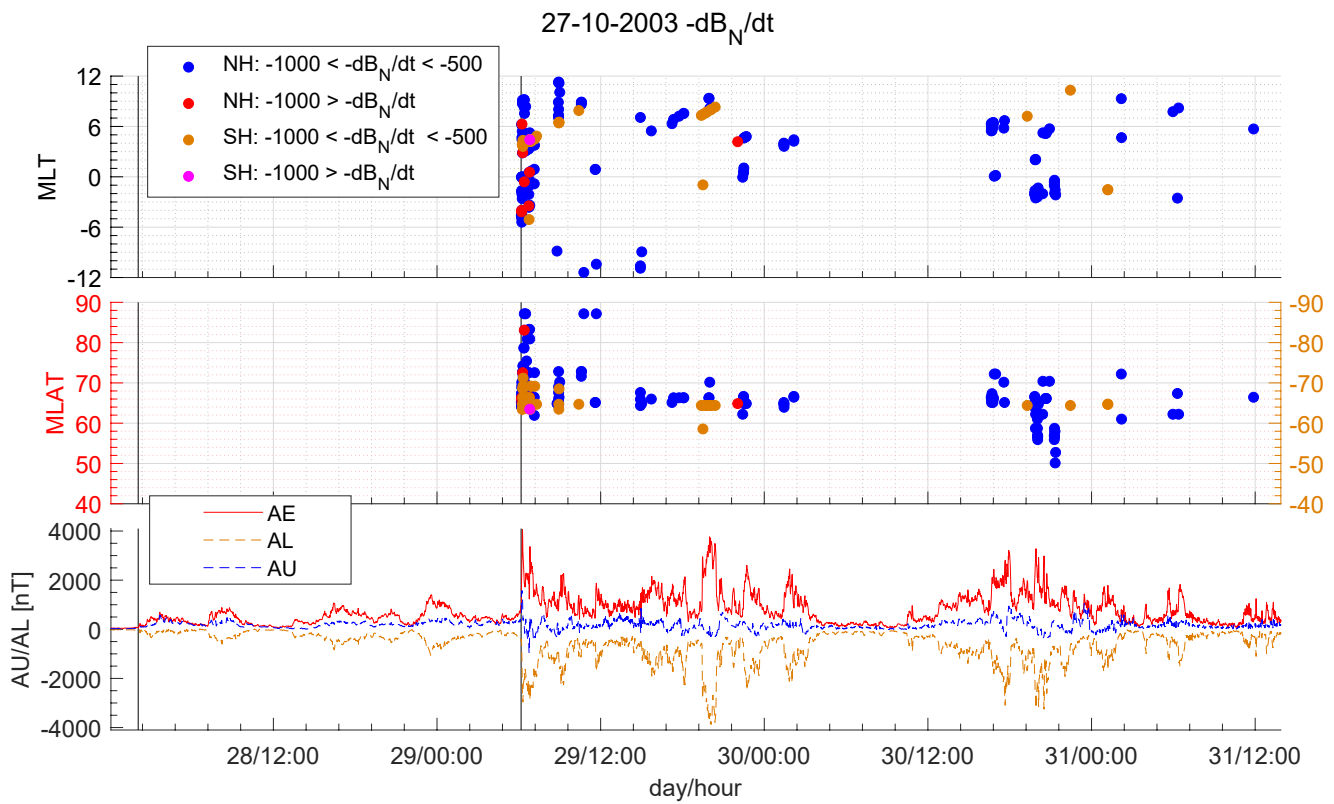


Figure 7. Similar as Figure 6 for the Halloween storm on 29 October 2003 storm.

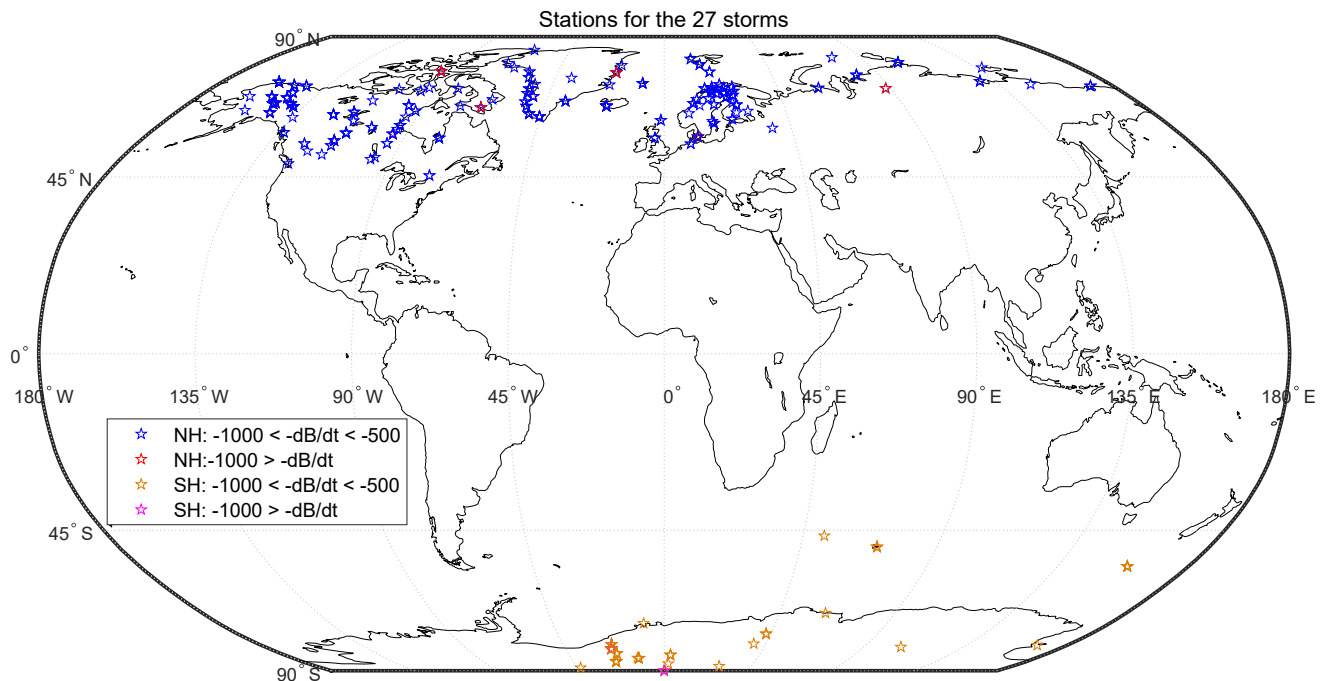


Figure 8. Spatial distribution of all stations that recorded one (or more) spikes during the 27 storms. The coverage between Europe and North-America is roughly similar.

**Table 1**  
*The 27 Storms With at Least 10 Recorded Spikes*

Number of spikes	Date	Av. Sta. <sup>a</sup>	Sta. with spikes <sup>b</sup>	Spikes/ Sta.
218	27 October 2003	201	66	3.3
59	26 July 2004	187	25	2.36
36	23 March 1991	80	18	2
34	2 September 2017	224	23	1.47
34	3 November 2004	207	26	1.3
33	8 February 1986	46	12	2.75
30	12 March 1989	58	14	2.14
29	11 September 2005	210	24	1.21
27	21 January 2005	216	13	2.1
27	24 July 2004	190	16	1.68
25	20 November 2003	202	11	2.27
22	14 December 2006	223	15	1.46
22	24 September 1998	160	14	1.57
21	15 July 2000	172	14	1.5
20	15 May 2005	210	16	1.25
19	29 May 2003	205	12	1.58
17	8 March 2012	261	13	1.31
17	24 November 2001	175	11	1.54
15	4 May 1998	163	12	1.25
15	13 July 1982	28	10	1.5
14	11 April 2001	181	8	1.75
14	21 February 1988	54	2	7
12	20 February 1994	106	9	1.33
11	23 August 2018	207	10	1.1
11	13 March 2015	229	9	1.22
11	17 June 2003	204	5	2.2
11	4 February 1983	37	6	1.83

*Note.* The first column gives the number of spikes that also corresponds to the X-axis in Figure 9, the last column gives the average of spikes per stations.

<sup>a</sup>Available stations by SuperMAG. <sup>b</sup>Stations that recorded at least one spike.

$dt < -1,000$  nT/min. Note that the more “bold/strong” the stars are, the more spikes have been recorded at these stations. The spatial distribution of the stations is similar around the world if we consider the number of stations available and where data are free for access. Finally, we also found that the number of dB/dt spikes is independent of the station distribution, see Table 1.

#### 4.4. Magnetic Indices and dB/dt Spikes

Kataoka and Ngwira (2016) identified three different types of GICs based on the timescale of dB/dt drivers: ring-current type characterized by a slow dB/dt (timescale of hours), auroral electrojets type characterized by a fast dB/dt (timescale of minutes), and SSC type characterized by a very fast dB/dt (timescale of seconds). The spikes analyzed in this study correspond mainly to dB/dt drivers associated with the auroral electrojets. According to Kataoka and Ngwira (2016) emergency framework (considering dB/dt spikes and also the Dst index), our extreme spikes fall within the caution level for the high latitude range. Moreover, Wu et al. (2004) and Engebretson et al. (2021) argued that the storm intensity does not influence the substorm development within the storm and subsequently the resulting spikes in the magnetic field. We agree with this hypothesis; considering the 27 storms with a minimum of 10 spikes, the strongest storm in intensity (according to Dst or AL index) is not necessarily associated with a storm with the highest number of spikes. Figure 9 displays the number of spikes (for each of the 27 storms) as a function of the Dst (left y axis—blue asterisks) and the AL (right y axis—red triangles) index. Neither the strongest Dst (−589 nT) nor the strongest AL (−5,636 nT) storms is linked to the storm with the highest number of spikes (218). This conclusion should be taken carefully because the peak value of the indices is for the entire storm period and thus not directly related to the occurrence period of dB/dt spikes. Additionally, Table 1 gives the average number of spikes per station that recorded at least one spike (see fifth column). The third and fourth columns provide the number of available stations by SuperMAG for the storm and the number of stations that recorded at least one spike respectively. Except for a few storms, the number of available stations does not necessary play a role; the storms with the higher number of spikes have a higher spike average per station.

The most intense storm according to Dst index (Dst = −589 nT) occurred 13 March 1989 (not shown in any of the figures), but had a corresponding AL index of −2,797 nT and features only 30 dB/dt spikes (2.14 average spikes per station, see Table 1). For this storm period, we identified two separate shifted spatiotemporal development sequences for the dB/dt spikes. According to the AL index, the most intense storm from our data set happened on

8 February 1986 (see Figure 5) with an AL index of −5,636 nT and Dst = −307 nT, for a similar number of dB/dt spikes (33 spikes, 2.75 in average, see Table 1) as the 13 March 1989 storm. Based on the results from Figure 9, we suggest that neither AL nor Dst index give any indication of how often, when and where the spikes occur. The Dst index contains little information about the danger of a storm for GIC as already suggested by Wu et al. (2004) and Yagova et al. (2018), it only gives a measure of the enhancement of the disturbances in the ring current throughout the entire storm. Moreover, as we showed in the previous storm examples, the spikes do follow to some extent the enhancement of the AU/AL index. A strong onset in the AL/AU index usually correspond to dB/dt spike(s) in a storm. This observation supports the result of Yagova et al. (2018) and Dimmock et al. (2020) (using IMAGE network) showing that the extreme dB/dt values occurrence is often closely related to the AE index. However, the AE index is not sensitive to dB/dt spikes equatorward of the nominal auroral oval. Therefore, the extreme dB/dt values should be better related to the SuperMAG SME index (Newell & Gjerloev, 2011), which uses many more stations than the original AE index (12 stations in auroral zone). A wider latitudinal coverage of magnetometer stations certainly will capture more intensification onsets. Concerning the Dst/SYM-H index, the

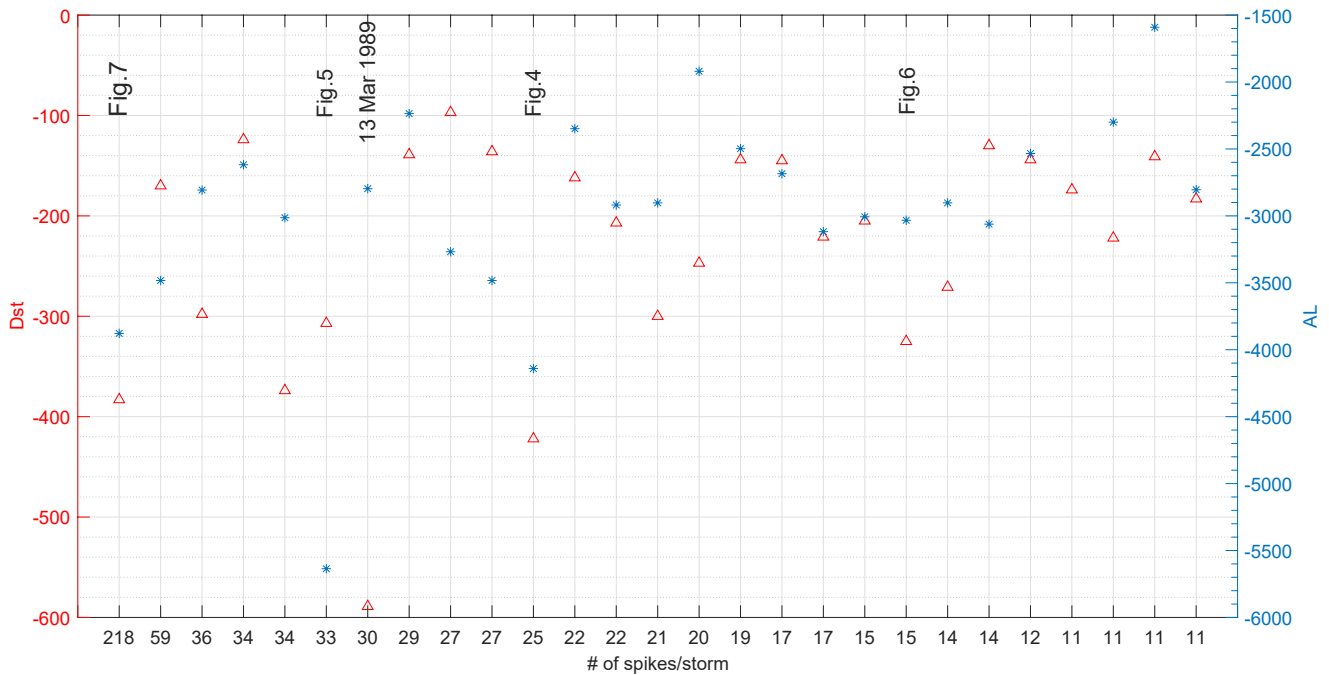


**Figure 9.** Number of spikes for each storm ( $x$  axis) compared to its corresponding minimum Dst (left  $y$  axis, red triangles) and AL index (right  $y$  axis, blue asterisks) during the storm period. The storm with the highest number of dB/dt spikes (218) is not associated with the most intense storms (Dst  $-589$  nT or AL  $-5,636$  nT depending on the index classification). The labels Figures 4–7 show the storms presented in the corresponding figures, while 13 March 1989 storm is discussed in the text.

strongest values do often coincide with the morning sector spikes, while the pre-midnight spikes, correspond to intensification in the early or main phase of a storm.

Both the AE index and the Dst/SYM-H index strongly depend on the solar drivers and in particular the direction of the IMF. Moreover, local changes of IMF or the solar wind dynamic pressure are not well reflected in the magnetic indices nor in the known energy coupling Epsilon parameter (Akasofu, 1981), which represents the total energy transfer from the solar wind into the magnetosphere. There might be changes in the solar wind hitting Earth that are not observed at L1 point. Thus, we suggest that a more subtle and local variability in the solar drivers could be the source of many dB/dt spikes detected in the magnetograms.

#### 4.5. dB/dt Spikes and Detrimental GICs

Detrimental GICs caused by dB/dt spikes as a primary drivers have been discussed and investigated by several studies for example, Pulkkinen and Kataoka (2006), Pulkkinen et al. (2008), Marshall et al. (2010), Grawe et al. (2018), Heyns et al. (2021), and Rogers et al. (2021). If and when coinciding with calamitous structures in the underlying ground conductivity and power network, rapid and short-lived geomagnetic variations lead to detrimental GICs. While the above studies suggest and highlight the importance of a frequency-weighted dB/dt spectrum and high resolution data, when looking at extreme geomagnetic storms, 1 min resolution data seem to be sufficient for the determination of geoelectric field enhancements as also done by Ngwira et al. (2013) and Ngwira et al. (2015). Our results confirm the importance of understanding the preferred MLT location of the dB/dt spikes, as well as the spatiotemporal evolution of the rapid time-varying dB/dt spikes during a storm. It is important to know where and when such disturbances are more likely to develop both in space and in time, as they may create potential detrimental GICs, when occurring in regions of certain features in the ground-conductivity or weak spots of regional power networks. Our findings deal mostly with the physical nature of rapid magnetic variations wherever they occur, without investigating the actual occurrence of GICs. From a magnetospheric point of view, the near-Earth magnetospheric-ionospheric coupling leading to large ionospheric currents and causes large GICs is still poorly understood (Schrijver et al., 2015). Thus, our results indicate that further knowledge on the cause and individual locations of substorm onsets, wedgelets and Omega bands based on dedicated



and detailed event studies on the occurrences of associated dB/dt spikes may help to improve the forecast of GICs. Warnings concerning “statistical hotspot” moving over a certain infrastructure network may be useful for operators. In comparison to general warnings concerning the entire period of a geomagnetic storm, the operators will be aware of potential dangerous specific periods during a given storm. From our data and results, we observed a certain amount of dB/dt spikes outside the two MLT hotspots. Thus, we conclude that more scientific effort is needed to better understand exactly where and when substorm-like features of SCW/WTS and Omega bands could occur in the extremely distorted magnetospheric environment, as they sometimes can occur outside the statistical limits. Based on such improved knowledge a future Space Weather observing network could be designed to deliver the necessary data to develop warning-systems precise enough to fulfill the requirements of end user needs (Schrijver et al., 2015).

## 5. Conclusions

We studied rapid dB/dt disturbances (with a threshold of  $|dB/dt| \geq 1500$  nT/min) for geomagnetic storms between 1980 and 2020 (storms list created by W. T. Walach with the algorithm described in Walach and Grocott [2019]). We analyzed the occurrences of dB/dt spikes for each storm and studied further into detail 27 storms with more than 10 detected spikes. Using a worldwide coverage of magnetometer stations in both hemispheres, we investigated negative and positive spikes in both the northern and eastern magnetic components. We confirmed two “hotspots” with a higher occurrence frequency of dB/dt spikes; one in the pre-midnight MLT sector and the second one in the dawn MLT sector. These hotspots had already been shown over Scandinavia and Canada (EPRI, 2020; Juusola et al., 2015; Kataoka & Pulkkinen, 2008; Viljanen et al., 2001; Weigel et al., 2002) but not for a simultaneous worldwide coverage. Additionally, we analyzed both east west and north south directed magnetic components independently. In the evening sector, the prominent negative X-component spikes are probably due to the onset of a SCW, and sometimes due to a westward traveling surge (WTS), when the negative dB/dt spikes in the northern component are observed simultaneously with positive eastward dB/dt spikes. In the morning sector, we suggested large scale undulations in the auroral electrojet, commonly known as Omega bands, as the most probable physical phenomenon behind the dB/dt spikes. Omega bands are commonly indicated by negative and positive spikes in both components.

Our main result shows a general spatiotemporal development of the negative northern dB/dt spikes for most of the geomagnetic storms within the subset of 27 storms. This subset consists of storms with more than 10 detected dB/dt spikes. During the period of a storm (or during any clearly discernible intensification of an ongoing storm), the location of the spikes developed from the pre-midnight sector (hotspot) toward the morning sector (hotspot), and the start of this development is often correlated with a clear onset in the AL index (see Figure 5). If several major AL-bursts occurred in the AE index within a storm, several temporal sequences could be observed for a single storm. As all storms have their own features, there are some exceptions for which multiple MLT sectors were activated either all at once or in different sequences including the dusk and pre-noon MLT sectors (see Figure 6). These multiple activations resulted in the detection of dB/dt spikes in sub-auroral magnetic latitudes (down to  $50^\circ$  rather than around the usual  $\sim 65^\circ$ ).

As a third result, we could show that the intensity of a storm, as defined by the Dst (SYM-H) or AE indices is not correlated with the number of featured dB/dt spikes. In other words, a major geomagnetic storm does not necessarily have a higher number of spikes than a moderate one. This non-correlation between the magnitude of the storm magnetic disturbance and its “spikyness” indicates in our opinion that the dB/dt spikes may be the consequence of a local variability in the solar drivers, or a local magnetospheric process. The local magnetospheric process may not be captured by the averaged magnetic indices or any of the general energy-coupling parameters. We plan a future study to identify any potential solar wind characteristics that may cause either “spiky” or smooth storms. This result is in agreement with the technical report from the Electrical Power Research Institute (US; EPRI, 2020), where the authors did not find a clear trend between the storm intensity and the direction or strength of dB/dt spikes.

We have shown that the statistical occurrence pattern of strong dB/dt spikes in the form of two hotspots is indeed a global and not a local phenomenon. Separating the disturbances in northern and eastern components, we suggest different physical mechanisms causing the hotspots, and we could also show that both hotspots activate at different times in the development of a storm. As the intensity of the storm measured by the AE and Dst indices

shows not correlation with the probability of spike occurrences, the dB/dt spikes do follow a temporal evolution while the storm is developing. Every new sequence is associated to a burst in the AE index. We therefore need to understand more about the detailed driving mechanisms for such spikes in the different storms. In the future, we plan to analyze the solar wind data for storms with high dB/dt occurrences and “smoother storms” in order to identify possible external driver mechanisms.

In future studies, we plan to use magnetic data with a higher time resolution (10 s or even 1 s data), to detect any spike events, which in our case may have fallen into two adjacent 1 min bins. Such higher resolution could also address more spectral details in the dB/dt variability, which have a strong impact on GIC occurrences as already pointed out by several studies (Grawe et al., 2018; Heyns et al., 2021; Marshall et al., 2010; Pulkkinen & Kataoka, 2006; Pulkkinen et al., 2008; Rogers et al., 2021). Both in the US and in Europe (through the European Space Agency that funded the MAG-SWE-DAN magnetometer project) such improved observational networks are being developed and their data will soon become available within the SuperMAG services. Once the full entity of such short-lived spikes in storms can truly and uniquely be detected and understood, one will need to correlate their refined occurrence statistics with a variety of solar wind drivers and internal magnetic processes, considering local effects whenever possible. It will then be possible to predict the occurrence of more dangerous storm periods, and eventually model the occurrence of individual extreme spikes.

### Conflict of Interest

The authors declare no conflicts of interest relevant to this study.

### Data Availability Statement

The authors first would like to thank M. T. Walach for providing the storms list 1980–2020 using her algorithm discussed in Walach and Grocott (2019). The authors thank the SuperMAG team for their services and time for discussing the data (<http://SuperMAG.jhuapl.edu/mag/>). The storm list and data set downloaded from SuperMAG can be accessed <https://doi.org/10.5281/zenodo.4922994>. The AE and SYM-H indices data were retrieved from the OMNIWeb page [https://omniweb.gsfc.nasa.gov/form/omni\\_min.html](https://omniweb.gsfc.nasa.gov/form/omni_min.html), the Dst data from the Kyoto page <http://wdc.kugi.kyoto-u.ac.jp/dst/dir/index.html> and the SSC data stem from the International Service of Geomagnetic Indices <http://www.obsebre.es/en/rapid>.

### Acknowledgments

A. Schillings and H. J. Opgenoorth acknowledge the Swedish National Space Agency (SNSA) for its financial support under the Grant 10077/15. Under the same SNSA Grant 10077/15, LP started the work with the IRF Uppsala affiliation until 2017. In 2019, A. Schillings took over the work. M. Hamrin was supported by the SNSA Grant 81/17 and the Swedish Research Council Grant 2018-03623.

### References

- Akasofu, S. I. (1981). Energy coupling between the solar wind and the magnetosphere. *Space Science Reviews*, 28(2), 121–190. <https://doi.org/10.1007/BF00218810>
- Apatenkov, S. V., Pilipenko, V. A., Gordeev, E. I., Viljanen, A., Juusola, L., Belakhovsky, V. B., et al. (2020). Auroral omega bands are a significant cause of large geomagnetically induced currents. *Geophysical Research Letters*, 47(6), e2019GL086677. <https://doi.org/10.1029/2019GL086677>
- Boteler, D. H. (2019). A 21st century view of the March 1989 magnetic storm. *Space Weather*, 17(10), 1427–1441. <https://doi.org/10.1029/2019SW002278>
- Cannon, P., Angling, M., Barclay, L., Curry, C., Dyer, C., Edwards, R., et al. (2013). *Extreme space weather: Impacts on engineered systems and infrastructure* (Technical Report). Royal Academy of Engineering.
- Dimmock, A. P., Rosenqvist, L., Welling, D. T., Viljanen, A., Honkonen, I., Boynton, R. J., & Yordanova, E. (2020). On the regional variability of dB/dt and its significance to GIC. *Space Weather*, 18(8), e2020SW002497. <https://doi.org/10.1029/2020SW002497>
- Ebihara, Y., & Tanaka, T. (2018). Why does substorm-associated auroral surge travel westward? *Plasma Physics and Controlled Fusion*, 60(1), 014024. <https://doi.org/10.1088/1361-6587/aa89fd>
- Echer, E., Gonzalez, W. D., Tsurutani, B. T., & Gonzalez, A. L. C. (2008). Interplanetary conditions causing intense geomagnetic storms (Dst ≤ −100 nT) during solar cycle 23 (1996–2006). *Journal of Geophysical Research*, 113(A5). <https://doi.org/10.1029/2007JA012744>
- Engebretson, M. J., Kirkeveld, K. R., Steinmetz, E. S., Pilipenko, V. A., Moldwin, M. B., McCuen, B. A., et al. (2020). Interhemispheric comparisons of large nighttime magnetic perturbation events relevant to GICs. *Journal of Geophysical Research: Space Physics*, 125(8), e2020JA028128. <https://doi.org/10.1029/2020JA028128>
- Engebretson, M. J., Pilipenko, V. A., Steinmetz, E. S., Moldwin, M. B., Connors, M. G., Boteler, D. H., et al. (2021). Nighttime magnetic perturbation events observed in Arctic Canada: 3. Occurrence and amplitude as functions of magnetic latitude, local time, and magnetic disturbance indices. *Space Weather*, 19(3), e2020SW002526. <https://doi.org/10.1029/2020SW002526>
- EPRI. (2020). *Furthering the understanding of the characteristics and scales of geoelectric field enhancements* (Technical Report). EPRI. 20203002017900
- Erinmez, I., Kappenman, J. G., & Radasky, W. A. (2002). Management of the geomagnetically induced current risks on the national grid company's electric power transmission system. *Journal of Atmospheric and Solar-Terrestrial Physics*, 64(5), 743–756. (Space Storms and Space Weather). [https://doi.org/10.1016/S1364-6826\(02\)00036-6](https://doi.org/10.1016/S1364-6826(02)00036-6)

- Gjerloev, J. W. (2012). The SuperMAG data processing technique. *Journal of Geophysical Research*, *117*(A9). <https://doi.org/10.1029/2012JA017683>
- Gonzalez, W. D., Joselyn, J. A., Kamide, Y., Kroehl, H. W., Rostoker, G., Tsurutani, B. T., & Vasyliunas, V. M. (1994). What is a geomagnetic storm? *Journal of Geophysical Research*, *99*(A4), 5771–5792. <https://doi.org/10.1029/93JA02867>
- Gonzalez, W. D., Tsurutani, B. T., Lepping, R. P., & Schwenn, R. (2002). Interplanetary phenomena associated with very intense geomagnetic storms. *Journal of Atmospheric and Solar-Terrestrial Physics*, *64*(2), 173–181. (STEP-Results, Applications and Modelling Phase (S-RAMP)). [https://doi.org/10.1016/S1364-6826\(01\)00082-7](https://doi.org/10.1016/S1364-6826(01)00082-7)
- Grawe, M. A., Makela, J. J., Butala, M. D., & Kamalabadi, F. (2018). The impact of magnetic field temporal sampling on modeled surface electric fields. *Space Weather*, *16*(11), 1721–1739. <https://doi.org/10.1029/2018SW001896>
- Heyns, M. J., Lotz, S. I., & Gaunt, C. T. (2021). Geomagnetic pulsations driving geomagnetically induced currents. *Space Weather*, *19*(2), e2020SW002557. <https://doi.org/10.1029/2020SW002557>
- Howard, T. A., & Menk, F. W. (2005). Ground observations of high-latitude Pc3–4 ULF waves. *Journal of Geophysical Research*, *110*(A4). <https://doi.org/10.1029/2004JA010417>
- Juusola, L., Viljanen, A., van de Kamp, M., Tanskanen, E. I., Vanhamäki, H., Partamies, N., & Kauristie, K. (2015). High-latitude ionospheric equivalent currents during strong space storms: Regional perspective. *Space Weather*, *13*(1), 49–60. <https://doi.org/10.1002/2014SW001139>
- Kamide, Y., Baumjohann, W., Daglis, I. A., Gonzalez, W. D., Grande, M., Joselyn, J. A., et al. (1998). Current understanding of magnetic storms: Storm-substorm relationships. *Journal of Geophysical Research*, *103*(A8), 17705–17728. <https://doi.org/10.1029/98JA01426>
- Kappenman, J. G. (2003). Storm sudden commencement events and the associated geomagnetically induced current risks to ground-based systems at low-latitude and midlatitude locations. *Space Weather*, *1*(3). <https://doi.org/10.1029/2003SW000009>
- Kappenman, J. G. (2006). Great geomagnetic storms and extreme impulsive geomagnetic field disturbance events – An analysis of observational evidence including the great storm of May 1921. *Advances in Space Research*, *38*(2), 188–199. <https://doi.org/10.1016/j.asr.2005.08.055>
- Kataoka, R., Fukunishi, H., Lanzerotti, L. J., MacLennan, C. G., Frey, H. U., Mende, S. B., et al. (2001). Magnetic impulse event: A detailed case study of extended ground and space observations. *Journal of Geophysical Research*, *106*(A11), 25873–25889. <https://doi.org/10.1029/2000JA000314>
- Kataoka, R., & Ngwira, C. (2016). Extreme geomagnetically induced currents. *Progress in Earth and Planetary Science*, *3*(1), 23. <https://doi.org/10.1186/s40645-016-0101-x>
- Kataoka, R., & Pulkkinen, A. (2008). Geomagnetically induced currents during intense storms driven by coronal mass ejections and corotating interacting regions. *Journal of Geophysical Research*, *113*(A3). <https://doi.org/10.1029/2007JA012487>
- Kepko, L., McPherron, R. L., Amm, O., Apatenkov, S., Baumjohann, W., Birn, J., et al. (2015). Substorm current wedge revisited. *Space Science Reviews*, *190*(1), 1–46. <https://doi.org/10.1007/s11214-014-0124-9>
- Kisabeth, J. L., & Rostoker, G. (1973). Current flow in auroral loops and surges inferred from ground-based magnetic observations. *Journal of Geophysical Research*, *78*(25), 5573–5584. <https://doi.org/10.1029/JA078i025p05573>
- Kleimenova, N. G., Gromova, L. I., Gromov, S. V., & Malysheva, L. M. (2018). Large magnetic storm on September 7–8, 2017: High-latitude geomagnetic variations and geomagnetic Pc5 pulsations. *Geomagnetism and Aeronomy*, *58*(5), 597–606. <https://doi.org/10.1134/S0016793218050080>
- Lakhina, G., & Tsurutani, B. (2016). Geomagnetic storms: Historical perspective to modern view. *Geoscience Letters*, *3*(5). <https://doi.org/10.1186/s40562-016-0037-4>
- Lyons, L. R., Nishimura, Y., Donovan, E., & Angelopoulos, V. (2013). Distinction between auroral substorm onset and traditional ground magnetic onset signatures. *Journal of Geophysical Research: Space Physics*, *118*(7), 4080–4092. <https://doi.org/10.1002/jgra.50384>
- Marshall, R. A., Waters, C. L., & Sciffer, M. D. (2010). Spectral analysis of pipe-to-soil potentials with variations of the Earth's magnetic field in the Australian region. *Space Weather*, *8*(5). <https://doi.org/10.1029/2009SW000553>
- McPherron, R. L. (1997). The role of substorms in the generation of magnetic storms. In *Magnetic storms* (pp. 131–147). American Geophysical Union. <https://doi.org/10.1029/GM098p0131>
- McPherron, R. L., Russell, C. T., & Aubry, M. P. (1973). Satellite studies of magnetospheric substorms on August 15, 1968: 9. Phenomenological model for substorms. *Journal of Geophysical Research*, *78*(16), 3131–3149. <https://doi.org/10.1029/JA078i016p03131>
- Newell, P. T., & Gjerloev, J. W. (2011). Evaluation of supermag auroral electrojet indices as indicators of substorms and auroral power. *Journal of Geophysical Research*, *116*(A12). <https://doi.org/10.1029/2011JA016779>
- Ngwira, C. M., Pulkkinen, A., Bernabeu, E., Eichner, J., Viljanen, A., & Crowley, G. (2015). Characteristics of extreme geoelectric fields and their possible causes: Localized peak enhancements. *Geophysical Research Letters*, *42*(17), 6916–6921. <https://doi.org/10.1002/2015GL065061>
- Ngwira, C. M., Pulkkinen, A., Wilder, F. D., & Crowley, G. (2013). Extended study of extreme geoelectric field event scenarios for geomagnetically induced current applications. *Space Weather*, *11*(3), 121–131. <https://doi.org/10.1002/swe.20021>
- Ngwira, C. M., Sibeck, D., Silveira, M. V. D., Georgiou, M., Weygand, J. M., Nishimura, Y., & Hampton, D. (2018). A study of intense local dB/dt variations during two geomagnetic storms. *Space Weather*, *16*(6), 676–693. <https://doi.org/10.1029/2018SW001911>
- Opgenoorth, H. J., Oksman, J., Kaila, K. U., Nielsen, E., & Baumjohann, W. (1983). Characteristics of eastward drifting omega bands in the morning sector of the auroral oval. *Journal of Geophysical Research*, *88*(A11), 9171–9185. <https://doi.org/10.1029/JA088iA11p09171>
- Opgenoorth, H. J., Persson, M. A. L., Pulkkinen, T. I., & Pellinen, R. J. (1994). Recovery phase of magnetospheric substorms and its association with morning-sector aurora. *Journal of Geophysical Research*, *99*(A3), 4115–4129. <https://doi.org/10.1029/93JA01502>
- Palin, L., Jacquey, C., Opgenoorth, H., Connors, M., Sergeev, V., Sauvaud, J.-A., et al. (2015). Three-dimensional current systems and ionospheric effects associated with small dipolarization fronts. *Journal of Geophysical Research: Space Physics*, *120*(5), 3739–3757. <https://doi.org/10.1002/2015JA021040>
- Palin, L., Opgenoorth, H. J., Ågren, K., Zivkovic, T., Sergeev, V. A., Kubysheva, M. V., et al. (2016). Modulation of the substorm current wedge by bursty bulk flows: 8 September 2002—Revisited. *Journal of Geophysical Research: Space Physics*, *121*(5), 4466–4482. <https://doi.org/10.1002/2015JA022262>
- Partamies, N., Weygand, J. M., & Juusola, L. (2017). Statistical study of auroral omega bands. *Annales Geophysicae*, *35*(5), 1069–1083. <https://doi.org/10.5194/angeo-35-1069-2017>
- Pirjola, R. (2000). Geomagnetically induced currents during magnetic storms. *IEEE Transactions on Plasma Science*, *28*(6), 1867–1873. <https://doi.org/10.1109/27.902215>
- Pirjola, R., & Boteler, D. (2002). Calculation methods of the electric and magnetic fields at the Earth's surface produced by a line current. *Radio Science*, *37*(3), 14–1–14–9. <https://doi.org/10.1029/2001RS002576>
- Pitout, F., & Bogdanova, Y. V. (2021). The polar cusp seen by cluster. *Journal of Geophysical Research: Space Physics*, *126*(9), e2021JA029582. <https://doi.org/10.1029/2021JA029582>
- Pulkkinen, A., & Kataoka, R. (2006). S-transform view of geomagnetically induced currents during geomagnetic superstorms. *Geophysical Research Letters*, *33*(12). <https://doi.org/10.1029/2006GL025822>

- Pulkkinen, A., Kuznetsova, M., Ridley, A., Raeder, J., Vapirev, A., Weimer, D., et al. (2011). Geospace environment modeling 2008–2009 challenge: Ground magnetic field perturbations. *Space Weather*, 9(2). <https://doi.org/10.1029/2010SW000600>
- Pulkkinen, A., Pirjola, R., & Viljanen, A. (2008). Statistics of extreme geomagnetically induced current events. *Space Weather*, 6(7). <https://doi.org/10.1029/2008SW000388>
- Rogers, N. C., Wild, J. A., Eastoe, E. F., & Hübert, J. (2021). Climatological statistics of extreme geomagnetic fluctuations with periods from 1 s to 60 min. *Space Weather*, 19(11), e2021SW002824. <https://doi.org/10.1029/2021SW002824>
- Schillings, A., Palin, L., Opgenoorth, H. J., Hamrin, M., Rosenqvist, L., Gjerloev, J., et al. (2021). Distribution and occurrence frequency of dB/dt spikes during magnetic storms 1980–2019 [Dataset]. <https://doi.org/10.5281/zenodo.4922994>
- Schrijver, C. J., Kauristie, K., Aylward, A. D., Denardini, C. M., Gibson, S. E., Glover, A., et al. (2015). Understanding space weather to shield society: A global road map for 2015–2025 commissioned by COSPAR and ILWS. *Advances in Space Research*, 55(12), 2745–2807. <https://doi.org/10.1016/j.asr.2015.03.023>
- Thomson, A. W. P., Dawson, E. B., & Reay, S. J. (2011). Quantifying extreme behavior in geomagnetic activity. *Space Weather*, 9(10). <https://doi.org/10.1029/2011SW000696>
- Tighe, W., & Rostoker, G. (1981). Characteristics of westward travelling surges during magnetospheric substorms. *Journal of Geophysics*, 50(1), 51–67.
- Torta, J. M., Serrano, L., Regué, J. R., Sánchez, A. M., & Roldán, E. (2012). Geomagnetically induced currents in a power grid of northeastern Spain. *Space Weather*, 10(6). <https://doi.org/10.1029/2012SW000793>
- Tsurutani, B. T., Gonzalez, W. D., Tang, F., & Lee, Y. T. (1992). Great magnetic storms. *Geophysical Research Letters*, 19(1), 73–76. <https://doi.org/10.1029/91GL02783>
- Vennerström, S., Lefevre, L., Dumbović, M., Crosby, N., Malandraki, O., Patsou, I., et al. (2016). Extreme geomagnetic storms – 1868–2010. *Solar Physics*, 291(5), 1447–1481. <https://doi.org/10.1007/s11207-016-0897-y>
- Viljanen, A., Nevanlinna, H., Pajunpää, K., & Pulkkinen, A. (2001). Time derivative of the horizontal geomagnetic field as an activity indicator. *Annales Geophysicae*, 19(9), 1107–1118. <https://doi.org/10.5194/angeo-19-1107-2001>
- Viljanen, A., & Pirjola, R. (1994). Geomagnetically induced currents in the Finnish high-voltage power system. *Surveys in Geophysics*, 15(4), 383–408. <https://doi.org/10.1007/BF00665999>
- Viljanen, A., & Tanskanen, E. (2013). High-latitude magnetic fields and their time derivatives: Interhemispheric similarities. *Earth Planets and Space*, 65(1), 45–49. <https://doi.org/10.5047/eps.2012.05.014>
- Walach, M.-T., & Grocott, A. (2019). SuperDARN observations during geomagnetic storms, geomagnetically active times, and enhanced solar wind driving. *Journal of Geophysical Research: Space Physics*, 124(7), 5828–5847. <https://doi.org/10.1029/2019JA026816>
- Weigel, R. S., Klimas, A. J., & Vassiliadis, D. (2003). Solar wind coupling to and predictability of ground magnetic fields and their time derivatives. *Journal of Geophysical Research*, 108(A7). <https://doi.org/10.1029/2002JA009627>
- Weigel, R. S., Vassiliadis, D., & Klimas, A. J. (2002). Coupling of the solar wind to temporal fluctuations in ground magnetic fields. *Geophysical Research Letters*, 29(19), 21-1–21-4. <https://doi.org/10.1029/2002GL014740>
- Wik, M., Pirjola, R., Lundstedt, H., Viljanen, A., Wintoft, P., & Pulkkinen, A. (2009). Space weather events in July 1982 and October 2003 and the effects of geomagnetically induced currents on Swedish technical systems. *Annales Geophysicae*, 27(4), 1775–1787. <https://doi.org/10.5194/angeo-27-1775-2009>
- Wu, C.-C., Liou, K., Lepping, R., & Meng, C.-I. (2004). Identification of substorms within storms. *Journal of Atmospheric and Solar-Terrestrial Physics*, 66(2), 125–132. (Space Weather in the Declining Phase of the Solar Cycle). <https://doi.org/10.1016/j.jastp.2003.09.012>
- Yagova, N. V., Pilipenko, V. A., Fedorov, E. N., Lhamdondog, A. D., & Gusev, Y. P. (2018). Geomagnetically induced currents and space weather: P13 pulsations and extreme values of time derivatives of the geomagnetic field's horizontal components. *Izvestiya, Physics of the Solid Earth*, 54(5), 749–763. <https://doi.org/10.1134/S1069351318050130>
- Zhang, J., Richardson, I. G., Webb, D. F., Gopalswamy, N., Huttunen, E., Kasper, J. C., et al. (2007). Solar and interplanetary sources of major geomagnetic storms ( $Dst \leq -100$  nT) during 1996–2005. *Journal of Geophysical Research*, 112(A11), A10102. <https://doi.org/10.1029/2007JA012321>